Laser magnetic resonance rotational spectroscopy of $^2\Sigma$ radicals: Ethynyl (CCH)

Richard J. Saykally and Leif Veseth[a)]
Department of Chemistry and Materials and Molecular Research Division of the Lawrence Berkeley Laboratory, University of California, Berkeley, California 94720

Kenneth M. Evenson
Time and Frequency Division, National Bureau of Standards, Boulder, Colorado 80302

(Received 1 August 1983; accepted 7 December 1983)

The first terrestrial measurement of the free ethynyl radical (CCH), made by far-infrared laser magnetic resonance, is described. The $N = 6 \rightarrow 7$ rotational transition was observed for the lowest vibrational level of the $^2\Sigma^+$ ground state. Because of the very weak spin coupling in this state, the LMR spectrum is complex and badly overlapped. A theoretical formalism for the prediction and analysis of such weakly coupled $^2\Sigma$ states is presented, in which frequencies, linewidths, and intensities of all transitions are computed as a function of magnetic flux density, and the total absorption coefficient is computed at each field point in order to simulate the magnetic resonance spectrum. This formalism is used to analyze the LMR spectra of CCH. A combined least squares analysis of existing microwave, astronomical, and LMR data was carried out to determine an improved set of molecular parameters for this important interstellar molecule.

I. INTRODUCTION

In recent years, mechanistic studies of the combustion of hydrocarbon fuels have affirmed the important roles of reactive intermediates formed by successive hydrogen abstractions, addition reactions, and accompanying decomposition reactions in the combustion processes. For example, the methyl, ethyl, propyl, etc. radicals formed by a single hydrogen abstraction from the respective parent saturated hydrocarbons are among the most abundant radicals involved in the combustion of these fuels, and figure prominently in the reaction kinetics for these processes.[1] There exists little or no information on the geometrical structures or electronic properties of most of these radicals, in spite of the fact that such information is essential if reliable microscopic models of the overall combustion processes are to be constructed. The reasons for this lack of data are simply the well-known difficulties inherent in measuring spectra of short-lived species in energetic media, such as flames and plasmas. While the sensitive and powerful magnetic resonance techniques of gas-phase EPR and laser magnetic resonance (LMR) have been successfully applied to the study of a variety of reactive paramagnetic radicals in the gas phase,[2] these methods have not been considered applicable to the largest class of combustion intermediates. Radicals formed by a single hydrogen abstraction from saturated fuels, as well as many others formed in subsequent combustion processes, possess orbitally nondegenerate doublet ground states with small splittings between the two spin components. The interaction responsible for the splittings ("spin-rotation" interaction) arises principally from second-order spin-orbit effects which, in turn, are small because of the small spin-orbit interaction in the carbon atom itself. In order for a molecule to possess electric dipole allowed rotational transitions which can be tuned by a magnetic field, the electronic spin or orbital angular momenta must be coupled to the molecular axis system. In nondegenerate doublet ground states it is only the weak spin-rotation interaction which effects this coupling; for the doublet hydrocarbon radicals just described, the Zeeman interaction quickly overcomes the weak spin-rotation coupling and the spin becomes "decoupled," i.e., precesses independently about the field. This is the "molecular Paschen–Bach" regime, in which only magnetic dipole transitions possess Zeeman tunability. This difficulty with rapid spin decoupling, accompanied by complicated level crossings and anticrossings in the transition region from coupled to decoupled spin behavior, has essentially precluded the use of gas-phase EPR and LMR techniques to study ground states of these weakly coupled hydrocarbon radicals. In this paper, we present a theoretical formalism for the prediction and analysis of magnetic resonance spectra of the simplest class of weakly coupled molecules—those with $^2\Sigma$ electronic ground states—and describe the use of this model to interpret the laser magnetic resonance rotational spectrum of the weakly spin-coupled $^2\Sigma^+$ ground state of the ethynyl radical (CCH).

The ethynyl radical is the simplest molecule containing the carbon–carbon triple bond. It is an important intermediate in the combustion and photolysis of acetylene and has been shown to be one of the most ubiquitous molecules found in interstellar clouds.[3–6] As a member of the isoelectronic series including C_2, CN, CO^+, N_2^+, HCN^+, and $HCCH^+$, ethynyl is also an important prototype for *ab initio* calculations of simple open-shell systems.[7–9] While terrestrial studies of ethynyl have been carried out in cryogenic matrices using EPR,[10,11] infrared,[12] and visible[11] spectroscopy, laboratory spectra of the free molecule eluded detection until 1978, when the observation of the $N = 6 \rightarrow 7$ pure rotational transition in the $X\,^2\Sigma^+$ ground state of the ethynyl radical was made with the far-infrared laser magnetic resonance technique.[13] A detailed analysis of these spectra was not possible until the development of the model described in this

[a)] On leave from The Department of Physics, University of Oslo, Oslo, Norway.

 0021-9606/84/062247-09$02.10

paper. Recently, the laboratory microwave rotational spectrum of CCH, generated in a dc discharge through acetylene, has been measured by Sastry *et al.*,[14] and the infrared absorption spectrum was measured under similar conditions by Carrick *et al.*[15] In the latter work, many of the lines observed by color center laser magnetic rotational spectroscopy were assigned to transitions between excited vibrational levels of the $A\ ^2\Pi$ and $X\ ^2\Sigma^+$ electronic states, but vibrational transitions within the ground state were not detected. In this paper, we present a detailed account of the laser magnetic resonance experiments and the results that were obtained from them.

II. EXPERIMENTAL

In far-infrared laser magnetic resonance spectroscopy, one generally observes electric dipole-allowed transitions between rotational states of a molecule having unpaired electrons. Magnetic tunability results from the spin and orbital magnetic moments of the unpaired electrons, and the electric dipole character of transitions depends on the parity alternation between rotational states. As discussed above, it is the coupling of the electronic angular momenta to the molecular axes that yields dipole allowed Zeeman-tunable rotational transitions. The $X\ ^2\Sigma$ state of CCH exhibits a particularly striking example of a weak spin-coupling mechanism, with the electron spin-nuclear rotation coupling ($\gamma N \cdot S$) being only a few tens of MHz for low J values.[6] Accordingly, this interaction is overcome even for low values of the magnetic field. In this limit, only magnetic dipole transitions with $\Delta M_s = \pm 1$ tune in the magnetic field. Consequently, CCH would be considered a poor candidate for a magnetic resonance study because at all but the lowest flux densities, one would expect to observe only very broad electric dipole features or very weak (and probably undetectable) magnetic dipole lines. The rotational spectrum of CCH was originally predicted from the constants of Tucker, Kutner, and Thaddeus[4] by assuming that the D_0 value was the same as for acetylene (0.0452 MHz). This calculation, although uncertain because of lack of precise knowledge of D_0, predicted a close coincidence between the $J = 13/2 \rightarrow 15/2$ transition and a known far-infrared laser line, giving a reasonable probability that the transition could be observed at flux densities below the threshold for Paschen–Bach behavior.

The NBS–Boulder optically pumped far-infrared laser magnetic resonance spectrometer used in this work has been described previously.[2] It consists of a far-infrared gain cell pumped transversely by a cw grating- and piezoelectrically tuned CO_2 laser with a single line power output of 30 W, and an intracavity sample region, which is located between the pole faces of a 37.5 cm electromagnet capable of producing fields up to 2.0 T. The gain cell and sample region are physically separated by a rotatable polypropylene beamsplitter, which also determines the polarization (σ or π) of the laser relative to the static magnetic field. Fluorine atoms were produced in a 2450 MHz discharge through a dilute ($\sim 1\%$) mixture of F_2 in He and were pumped down the inner tube of a concentric flow reactor. A reactant gas was added through the outer reactor tube, producing a flame in the homogeneous field region of the sample cavity. As a rotational transition is tuned into resonance with the FIR laser frequency, the total power inside the laser cavity changes and is modulated at 5 kHz by a set of Helmholtz coils. The output of the laser is coupled into a helium-cooled germanium bolometer with a 45° cylindrical copper mirror 6 mm in diameter which is inserted the optimum distance into the laser mode pattern. The detector output is preamplified and fed into a lock-in amplifier. The demodulated output signal, observed on an XY recorder, approximates the first derivative of the absorption spectrum as a function of magnetic flux density.

Transitions attributable to CCH that occurred near zero flux density were first observed with the 490 μm laser line of vinyl bromide,[16] pumped by the 10P16 line of a CO_2 laser, in a flame generated by the reaction of fluorine atoms with ethane. It was subsequently found that essentially the same fluorine atom–methane flame[2] used to generate C, CH, CH_2, CH_2F, and CF produced these CCH signals with much greater intensity. The 490 μm LMR spectrum observed in the optimized flame is shown in Fig. 1 for both polarizations. A search of flux densities as high as 2.0 T revealed no additional features.

The chemistry of the carrier of the low field lines (five in π polarization and one in σ) was investigated. The signals were found to disappear when CH_4 was replaced by CD_4. Replacement of $^{12}CH_4$ by 90% $^{13}CH_4$ was found to extinguish the laser, due to a fortuitous coincidence with an unknown diamagnetic absorber. By reducing the fraction of ^{13}C in the CH_4 reactant, the quantitative dependence of the signal on $^{13}CH_4$ fraction was determined in a series of relative intensity measurements. For example, when $^{12}CH_4$ was replaced by a mixture of 80% $^{12}CH_4$ and 20% $^{13}CH_4$, the signal decreased by 64%, confirming the existence of two carbon atoms in the carrier of the spectrum. Similarly, replacement of CH_4 by CD_3H resulted in exactly a factor of 4 reduction in the spectral intensity, indicative of the presence of one hydrogen in the radical. The signal was then observed, albiet rather weakly, in a flame made by reacting oxygen atoms with acetylene, proving the absence of fluorine in the species. No spectra were observed upon addition of air or nitrogen to the flame. It was therefore concluded that the spectrum shown in Fig. 1 was due to the ethynyl radical.

Alternative sources of CCH were examined. It was found that reactions of F atoms with methanol, ethanol,

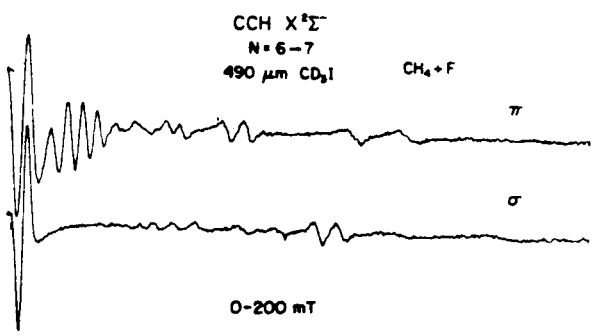

FIG. 1. The laser magnetic resonance spectrum observed for the $N = 6 \rightarrow 7$ transition of CCH with the 490 μm laser line of CD_3I. Only the strong lines at low fields (4 for π, 1 for σ) are due to this transition; the others are unassigned. See the text for details. (1 mT = 10 G).

acetylene, ethylene, ethane, and methane all produced CCH spectra, with methane still overwhelmingly producing the strongest lines.

The sign of the Zeeman tuning ($\partial B/\partial \nu_L$) was then determined for each line by shifting the laser to slightly higher (blue shift) or lower (red shift) frequencies, achieved by changing the FIR laser cavity length and observing the corresponding shift in the resonant fields. It was found that the strong feature at nearly zero field shifted to lower fields with a red laser shift ($\partial B/\partial \nu_L < 0$), while the four weaker components in the π spectrum behaved oppositely ($\partial B/\partial \nu_L < 0$).

The pressure was then reduced as low as possible with the CH_4–F source in order to achieve the highest resolution. It immediately became clear that each of the five observed "lines" were, in fact, superpositions of several transitions. It was found that at the lowest pressures used (8.0 Pa) a fluorine atom–ethane flame gave the most intense spectra. The best resolution was achieved in this case. In scanning to higher flux densities (0.3 T) a number of relatively sharp new lines were discovered with this low-pressure source. Frequency pulling experiments established that most of these lines were not related members of Zeeman sequences, but rather seemed to originate from several distinct transitions. Magnetic flux densities were measured with an accuracy of $\pm$ 0.1 mT directly from the field controller, which had been calibrated with a proton NMR Gauss meter.

III. THEORY

A. Fine structure and hyperfine structure of $^2\Sigma$ states

The Hamiltonian of a diatomic molecule or a nondegenerate state of a linear three-atomic molecule can be expressed as[17,18]

$$H = H_{ev} + H_{hf} + B\,\mathbf{F}^2 + B\,\mathbf{F}_a^2 - 2B\,\mathbf{F}\cdot\mathbf{F}_a\,, \tag{1}$$

where H_{ev} denotes the electronic and vibrational contributions, inclusive of spin-dependent and other relativistic effects. The term H_{hf} represents the hyperfine Hamiltonian, and $\mathbf{F}$ is the total angular momentum inclusive of nuclear spin, whereas $\mathbf{F}_a$ is given by

$$\mathbf{F}_a = \mathbf{L} + \mathbf{S} + \mathbf{I} = \mathbf{J}_a + \mathbf{I}\,. \tag{2}$$

It is convenient to rewrite the term $B\,\mathbf{F}_a$ of the Hamiltonian as

$$B\,\mathbf{F}_a^2 = B\,\mathbf{J}_a^2 + B\,\mathbf{I}^2 + 2B\,\mathbf{J}_a\cdot\mathbf{I}\,, \tag{3}$$

and to include the first two terms $B\,\mathbf{J}_a^2 + B\,\mathbf{I}^2$ in H_{ev}, since they will not couple electronic states of different symmetries.

The basis set used to solve the Schrödinger equation associated with the Hamiltonian of Eq. (1) was chosen in previous work[17,18] to be the linear combination of states which are fully coupled in the molecular axis system

$$|\psi^{\pm}_{q\Omega\Omega_I F M_F}\rangle = \frac{1}{\sqrt{2}}\left(|q\Omega\Omega_I I F M_F\rangle \pm (-1)^{F+S_q}|q-\Omega-\Omega_I I F M_F\rangle\right), \tag{4}$$

where Ω and Ω_I are the quantized components of $\mathbf{J}_a$ and $\mathbf{I}$, respectively, along the internuclear axis. In the present investigation, only one nucleus is assumed to have a nonzero nuclear spin, such that the total nuclear spin will be a good quantum number. The basis states of Eq. (4) are parity conserving eigenstates with the upper sign corresponding to + parity, and the lower sign to − parity. The phase factor S_q is a constant for a given electronic state and has the values $-I \mp \frac{1}{2}$ for $^2\Sigma^{\pm}$ states.

Although a $^2\Sigma$ state is clearly not best described to first order with the angular momenta fully coupled in the molecular frame, there are definite computational advantages for choosing such a basis. With any reasonable basis set, one certainly will have to go beyond the first-order description to adequately describe the results from high precision spectroscopy, such as LMR or EPR. Hence a secular equation will have to be diagonalized, and it will be roughly of the same size irrespective of the choice of basis set. Consequently, it is more expedient to employ a basis set which yields simple matrix elements which are easily derived, rather than one for which the diagonal elements happen to resemble the true eigenvalues.

The matrix elements of the Hamiltonian of Eq. (1) in the basis of Eq. (4) have been given previously for the general case[17,18] and only the specific elements relevant to a $^2\Sigma$ state are reproduced here. They are

$$\begin{aligned}\langle\psi^{\pm}_{q\Omega=1/2\Omega_I F}|H|\psi^{\pm}_{q\Omega=1/2\Omega' F}\rangle = {} & \{E + B\,[F(F+1) + \Omega_I - 2(\Omega_I+\tfrac{1}{2})^2]\}\delta_{\Omega,\Omega'} \\ & - B\,[(I+\Omega_I)(I-\Omega_I+1)(F+\tfrac{1}{2}+\Omega_I)(F-\Omega_I+\tfrac{1}{2})]^{1/2}\delta_{\Omega_I-1,\Omega'} \\ & \pm(-1)^{F+S_q}\langle q\Omega=\tfrac{1}{2}|BJ_{a+}|q\Omega=-\tfrac{1}{2}\rangle\{[(I+\Omega_I+1)(I-\Omega_I)]^{1/2}\delta_{\Omega_I+1,-\Omega'} \\ & - [(F+\Omega_I+\tfrac{1}{2})(F-\Omega_I+\tfrac{1}{2})]^{1/2}\delta_{\Omega',-\Omega}\} \\ & + \{\tfrac{1}{2}(b+c)\Omega_I + [3eQq_0/4I(2I-1)]\Omega_I^2\}\delta_{\Omega,\Omega'} \\ & \pm(-1)^{F+S_q}\tfrac{1}{2}b\,[(I+\Omega_I+1)(I-\Omega_I)]^{1/2}\delta_{\Omega_I+1,-\Omega'}\,.\end{aligned} \tag{5}$$

The range of Ω_I is given by

$$\max(-F-\tfrac{1}{2}, -I) \le \Omega_I \le \min(F-\tfrac{1}{2}, I).$$

In Eq. (5) E represents the electronic and vibrational energy, B the rotational constant, b and c are the standard Frosch and Foley magnetic hyperfine parameters, and eQq_0 is the quadrupole constant which applies only for $I > \frac{1}{2}$. The nonstandard parameter

$$\langle q\Omega=\tfrac{1}{2}|BJ_{a+}|q\Omega=-\tfrac{1}{2}\rangle$$

contained in Eq. (5) is easily evaluated in terms of the Hund's case (a) approximation to the general basis set of Eq. (4). For

a nonrotating molecule, the case (a) states are coupled by the spin-orbit interaction $\mathbf{AL}\cdot\mathbf{S}$, and the following relation is valid to second order:

$$|q\Omega = \tfrac{1}{2}\Omega_I IFM_F\rangle = |^2\Sigma v\Omega_I IFM_F\rangle + \sum_{^2\Pi,v'} \frac{\langle ^2\Pi v'|AL_+|^2\Sigma v\rangle}{2(E_{\Sigma v} - E_{\Pi v'})} |^2\Pi_{1/2} v'\Omega_I IFM_F\rangle . \quad (6)$$

By use of Eq. (6) one then obtains

$$\langle q\Omega = \tfrac{1}{2}|BJ_{a+}|q\Omega = -\tfrac{1}{2}\rangle = B - \tfrac{1}{2}\gamma_s \quad (7)$$

and

$$\gamma_s = 2\sum_{^2\Pi v'} \frac{\langle ^2\Pi v'|BL_+|^2\Sigma v\rangle\langle ^2\Pi v'|AL_+|^2\Sigma v\rangle}{E_{\Pi v'} - E_{\Sigma v}}, \quad (8)$$

where γ_s is recognized as the standard second-order spin-orbit contribution to the spin rotation constant $\gamma = \gamma^{(1)} + \gamma_s$ normally included by the effective Hamiltonian $\gamma\,\mathbf{N}\cdot\mathbf{S}$. The first order contribution $\gamma^{(1)}$ is expected to be negligible. By using the present coupled basis set, any spin-orbit dependent effects will be included to all orders in the effective parameters of the secular matrix.

The matrix elements of the hyperfine Hamiltonian are particularly simple in the present coupled basis set [cf. Eq. (5)]. In addition, the troublesome $\Delta J = \pm 1$ hyperfine elements encountered in the widely used case (a) and (b) decoupled basis sets are automatically included.

The matrix elements of Eq. (5) do not include interactions with other electronic states induced by the rotation of the molecule (Coriollis interaction). A Van Vleck transformation to second order would easily remedy this deficiency, but is, however, of minor interest since the result would only be a small correction term added to the rotational constant (electronic contribution to the moment of inertia).

The centrifugal distortion correction to the rotational energy is most easily included by squaring the rotational part of the secular matrix with the rotational constant B removed. The resulting matrix is then multiplied by the centrifugal distortion constant D and subtracted from the secular matrix.

B. The Zeeman effect of $^2\Sigma$ states

The interaction with an external magnetic field $\mathbf{B}$ is expressed by the Zeeman Hamiltonian

$$H_Z = \mu_B(g_l\mathbf{L} + g_s\mathbf{S} - g_I\mathbf{I})\cdot\mathbf{B} \quad (9)$$

when the contribution from the magnetic moment of the rotating nuclear charges is neglected. The matrix elements of the Zeeman Hamiltonian are described in detail in a previous paper.[18] The general result for the coupled basis set $|q\Omega\Omega_I IFM_F\rangle$ may be expressed in the following compact form:

$$\begin{aligned}\langle q\Omega\Omega_I IFM_F|H_Z|q'\Omega'\Omega_I' IF'M_F\rangle = \mu_B^B \sum_{\mu=-1}^{1} &\left[g_l\langle q\Omega|L_\mu|q'\Omega'\rangle\delta_{\Omega_I\Omega_I'} + g_s\langle q\Omega|S_\mu|q'\Omega'\rangle\delta_{qq'}\delta_{\Omega_I\Omega_I'} - g_I\langle q\Omega\Omega_I|I_\mu|q'\Omega'\Omega_I'\rangle\delta_{qq'}\delta_{\Omega\Omega'}\right] \\ &\times(-1)^{M_F-\Omega'-\Omega_I'-\mu}[(2F+1)(2F'+1)]^{1/2} \\ &\times\begin{pmatrix} F & 1 & F' \\ (\Omega+\Omega_I) & -\mu & -(\Omega'+\Omega_I')\end{pmatrix}\begin{pmatrix} F & 1 & F' \\ M_F & 0 & -M_F\end{pmatrix}. \end{aligned} \quad (10)$$

Here μ denotes the spherical molecule fixed components of the vectors $\mathbf{L}$, $\mathbf{S}$, and $\mathbf{I}$. Matrix elements for the parity eigenstates of Eq. (4) are readily obtained from Eq. (10). For a $^2\Sigma$ state it is sufficient to consider only $q = q'$ and $\Omega = \frac{1}{2}$, and the second order coupling case (a) approximation of Eq. (6) is used to evaluate the matrix elements of L_μ and S_μ. The results are

$$\begin{aligned}&\langle q\Omega = \tfrac{1}{2}|S_\mu|q\Omega'\rangle = \langle q\Sigma = \tfrac{1}{2}|S_\mu|q\Sigma'\rangle, \\ &\langle q\Omega = \tfrac{1}{2}|L_\mu|q\Omega = \tfrac{1}{2}\rangle = 0, \\ &\langle q\Omega = \tfrac{1}{2}|L_+|q\Omega = -\tfrac{1}{2}\rangle = g_A \\ &\quad = \sum_{^2\Pi,v'} \frac{\langle ^2\Pi v'|AL_+|^2\Sigma v\rangle\langle ^2\Pi v'|L_+|^2\Sigma v\rangle}{E_{\Sigma v} - E_{\Pi v'}}, \end{aligned} \quad (11)$$

and the second-order spin-orbit dependent g factor g_A is, as expected, included in the general matrix elements of Eq. (10).

The electronic orbital part of the Zeeman Hamiltonian also couples different electronic states. Another second-order g factor g_R' results from considering second-order cross terms between the Zeeman interaction $\mu_B g_l\mathbf{L}\cdot\mathbf{B}$ and the rotational Hamiltonian. For a $^2\Sigma$ state, g_R' is defined by

$$g_R' = -2g_l\sum_{^2\Pi,v'} \frac{\langle ^2\Pi v'|BL_+|^2\Sigma v\rangle\langle ^2\Pi v'|L_+|^2\Sigma v\rangle}{E_{\Sigma v} - E_{\Pi v'}} \quad (12)$$

and this g factor accounts for the electronic contribution to the total molecular rotational magnetic moment. This effect is explicitly included by adding an effective term $\mu_B g_R'\mathbf{R}\cdot\mathbf{B}$ to the Hamiltonian of Eq. (9), where $\mathbf{R}$ is the angular momentum of the nuclei. The Zeeman effect of $^2\Sigma$ states has also been considered recently by Raab *et al.*[19] who used a decoupled basis set to derive similar expressions for the second-order terms g_A and g_R'.

C. Relative intensities

The intensity of an electric dipole transition between states $|\psi'\rangle$ and $|\psi\rangle$ is proportional to the square of the matrix element of a space fixed spherical component d_μ of the electric dipole moment, i.e., to $|\langle\psi'|d_\mu|\psi\rangle|^2$. The state $|\psi\rangle$ of a molecule in an external magnetic field is expanded in the coupled basis of Eq. (4):

$$|\psi^\pm\rangle = \sum_{\Omega,\Omega_I,F} c^\pm_{q\Omega\Omega_I FM_F}|\psi^\pm_{q\Omega\Omega_I FM_F}\rangle . \quad (13)$$

The relative intensities of the lines for a transition from an upper vibronic state q' to a lower state q and a polarization determined by μ are given by

$$I_\mu = \left| \sum_{\Omega',\Omega_I',F'} \sum_{\Omega,\Omega_I,F} c^{\pm *}_{q'\Omega\Omega_I'F'M_F'} c^{\mp}_{q\Omega\Omega_IFM_F} \langle \psi^{\pm}_{q'\Omega'\Omega_I'F'M_F'} | d_\mu | \psi^{\mp}_{q\Omega\Omega_IFM_F} \rangle \right|^2 . \tag{14}$$

The matrix elements of the space fixed components d_μ must be expressed in terms of the molecule fixed axes; the result is

$$\langle q'\Omega'\Omega_I'F'M_F' | d_\mu | q\Omega\Omega_IFM_F \rangle = \sum_{\mu'=-1}^{1} \langle q'\Omega' | d_{\mu'} | q\Omega \rangle (-1)^{M_F-\Omega-\Omega_I+\mu-\mu'} \times [(2F'+1)(2F+1)]^{1/2} \begin{pmatrix} F' & 1 & F \\ \Omega'+\Omega_I' & -\mu' & -(\Omega+\Omega_I) \end{pmatrix} \begin{pmatrix} F' & 1 & F \\ M_F' & -\mu & -M_F \end{pmatrix}, \tag{15}$$

where $d_{\mu'}$ denotes molecule fixed spherical components. The case (a) approximation to the present coupled basis set is adequate for calculating matrix elements of the electric dipole moment operator $d_{\mu'}$, i.e., $|q\Omega\rangle = |q\Lambda\Sigma\rangle$ may be inserted in Eq. (15). For a rotational transition in a $^2\Sigma$ state, one then finally obtains the following expression for the relative intensities of the various lines split by fine structure, hyperfine structure, and an external magnetic field

$$I_\mu = |\langle q'\Lambda = 0\Sigma = \tfrac{1}{2}|d_0|q\Lambda = 0\Sigma = \tfrac{1}{2}\rangle|^2 \times \left| \sum_{\Omega_I,F,F'} c^{\pm}_{q'\Omega=1/2\,\Omega_I,F'M_F'} c^{\mp}_{q\Omega=\frac{1}{2}\Omega_I,FM_F} \times (-1)^{M_F-1/2-\Omega_I+\mu} [(2F'+1)(2F+1)]^{1/2} \begin{pmatrix} F' & 1 & F \\ \Omega_I+\frac{1}{2} & 0 & -\Omega_I-\frac{1}{2} \end{pmatrix} \begin{pmatrix} F' & 1 & F \\ M_F' & -\mu & -M_F \end{pmatrix} \right|^2 . \tag{16}$$

In Eq. (16), $\mu = \pm 1$ corresponds to circularly polarized radiation with selection rule $M_F' = M_F \pm 1$, and $\mu = 0$ corresponds to linear polarization with selection rule $M_F' = M_F$. Numerical values of the coefficients of Eq. (16) are obtained from the diagonalization of the secular matrix.

IV. ANALYSIS

A. Assignment of the spectrum

To assign the LMR spectrum of the $^2\Sigma$ electronic ground state of CCH, it will be useful to consider energy levels and transition frequencies with a simplified Hamiltonian[20]

$$H^0 = B\,\mathbf{N}^2 + \gamma \mathbf{N}\cdot\mathbf{S} + \mu_B g_s \mathbf{S}\cdot\mathbf{B} . \tag{17}$$

For strong fields, in which the contribution from the spin-rotation term is much less than that from the Zeeman interaction, the components of N and S along the external field will be quantized with quantum numbers M_N and M_S, respectively, and the energies are accordingly given by

$$E^0 = BN(N+1) + \gamma M_N M_S + \mu_B g_S B M_S . \tag{18}$$

Hence, the frequencies for allowed electric dipole transitions from rotational level N to $N+1$ are given in the strong field limit as

$$\Delta\nu_{\Delta M=0} = 2B(N+1), \qquad \Delta\nu_{\Delta M=\pm 1} = 2B(N+1) \pm \gamma M_S . \tag{19}$$

Consequently, no electric dipole allowed LMR spectrum will be observed for strong fields, since the transition frequencies are independent of the external field. For the present example, with $\gamma \simeq -60$ MHz, it follows from Eq. (18) that the transition towards the strong field case will be substantial for fields as low as a few hundred Gauss.

Figure 2 shows the zero-field $N=6$ and $N=7$ rotational energy level diagram for the $X\,^2\Sigma^+$ state of CCH, with the four strong zero-field transitions indicated. Frequencies for the $N=7$–6 transition were computed for various field strengths by use of molecular parameters from the microwave and astrophysical spectra, and with $g_s = 2.002\,319$, $g_l = 0.003\,042$, and $g_A = g_R' = 0.0$ [cf. Eqs. (10)–(12)]. For low fields, transition frequencies from the $J' = 6\frac{1}{2} - J'' = 5\frac{1}{2}$ transition were found to be in close coincidence with the laser frequency $\nu_L = 611\,333.6$ MHz, as shown in Fig. 3, for transitions with $\Delta M_F = 0$. Figure 3 also indicates that the proton hyperfine splitting in CCH will be difficult to resolve in the LMR spectrum. An assignment of the strong low-field lines for the $\Delta M_F = 0$ spectrum of Fig. 1 becomes rather straightforward with inspection of Fig. 3. The peak of 42 G is due to several overlapping lines, with no detailed assignment is made for it. The peaks at 102 and 175 G are easily assigned to transitions that are allowed in the low-field limit, whereas the assignment of the 230 and 274 G peaks involves lines that are very weak in this limit. The final assignments are given in Table I.

The single low-field peak in the $M_F = \pm 1$ spectrum is caused by many overlapping lines from the $J' = 6\frac{1}{2} - J'' = 5\frac{1}{2}$ transition with $M_F' - M_F'' = -1$. No detailed assignment of the individual components is possible.

B. Relative intensities in the CCH LMR spectrum

A synthesized LMR spectrum may be computed from Eq. (16) and the simplified Van Vleck–Weisskopf formula for the shapes of pressure broadened lines[20]

$$\gamma(\nu) = \frac{8\pi^2 Nf}{3ckT} I_\mu \frac{\nu^2 \Delta\nu}{(\nu-\nu_0)^2 + (\Delta\nu)^2} . \tag{20}$$

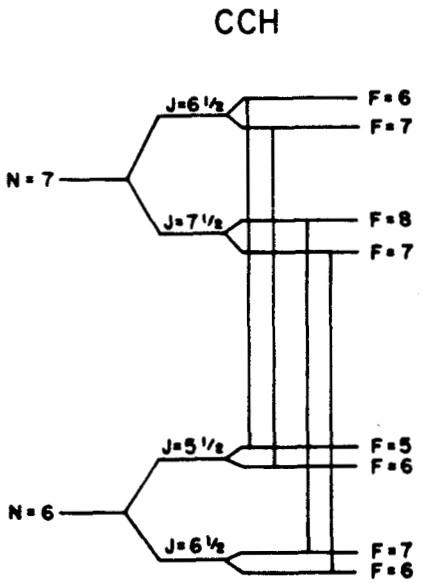

FIG. 2. Zero-field rotational energy level diagram for the $N = 7$ and $N = 6$ states of $X\,^2\Sigma$ CCH. The various splittings are not drawn to scale.

A computer program was written to compute the transition frequencies (ν_0) of all $N' = 7 - N'' = 6$ transitions with the corresponding values of I_μ at various field strengths. The contributions to γ at the laser frequency $\nu = 611\,333.6$ MHz from all possible resonance frequencies ν_0 were thereby obtained, and then summed at each field strength to yield the total absorption coefficient. The derivative of the total ab-

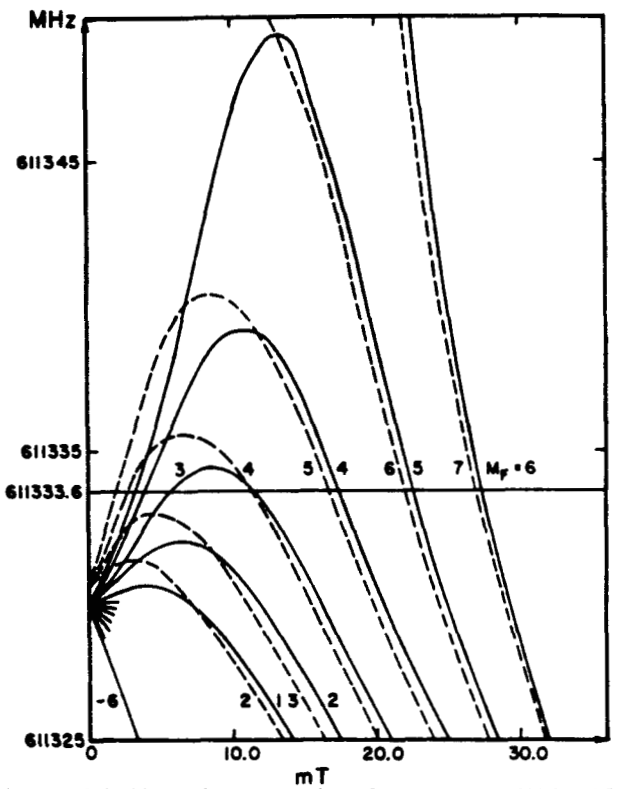

FIG. 3. Coincidences between the laser frequency $\nu_L = 611\,333.6$ MHz and transition frequencies for the $N = 7$–$N = 6$ for rotational transitions in the $^2\Sigma$ ground state of CCH as a function of magnetic field. The transitions shown are for $\Delta M_F = 0$, with the M_F value indicated along the horizontal line. Complete assignments are given in Table I.

TABLE I. Assignment of the CCH $\Delta M_F = 0$ LMR spectrum in terms of low-field quantum numbers (cf. Fig. 2). σ indicates the estimated uncertainty of the line with weight $1/\sigma^2$. The table also shows the microwave and astrophysical lines included in the fit.

N'	N''	J'	J''	F'	F''	M_F'	M_F''	$B(mT)$	Obs(MHz)	Obs–Calc(MHz)	σ
7	6	6½	5½	6	5	4	4				
7	6	6½	5½	7	6	3	3	10.2	611 333.6	−0.70	2.0
7	6	6½	5½	6	5	5	5				
7	6	6½	5½	7	6	4	4	17.5	611 333.6	0.13	1.0
7	6	6½	5½	6	6	6	6				
7	6	6½	5½	7	6	5	5	23.0	611 333.6	0.87	1.0
7	6	6½	6½	7	7	7	7				
7	6	6½	6½	7	7	6	6	27.4	611 333.6	0.05	1.0
4	3	4½	3½						349 338.10	0.29	0.50[a]
4	3	3½	2½						349 400.61	0.09	0.50[a]
3	2	3½	2½	4	3				262 004.260	−0.015	0.02[a]
3	2	3½	2½	3	2				262 006.482	0.011	0.02[a]
3	2	2½	1½	3	2				262 064.986	0.004	0.02[a]
3	2	2½	1½	2	1				262 067.469	−0.012	0.02[a]
2	1	2½	1½	3	2				174 663.179	0.007	0.02[a]
2	1	2½	1½	2	1				174 667.642	0.004	0.02[a]
2	1	1½	½	2	1				174 721.765	0.004	0.02[a]
2	1	1½	½	1	0				174 728.047	0.001	0.02[a]
1	0	1½	½	2	1				87 317.23	0.37	0.30[b]
1	0	1½	½	1	0				87 328.92	0.32	0.30[b]
1	0	½	½	1	1				87 402.34	0.37	0.30[b]
1	0	½	½	0	1				87 407.46	0.11	0.30[b]

[a] Sastry *et al.* (Ref. 14).
[b] Tucker, Kutner, and Thaddeus (Ref. 4).

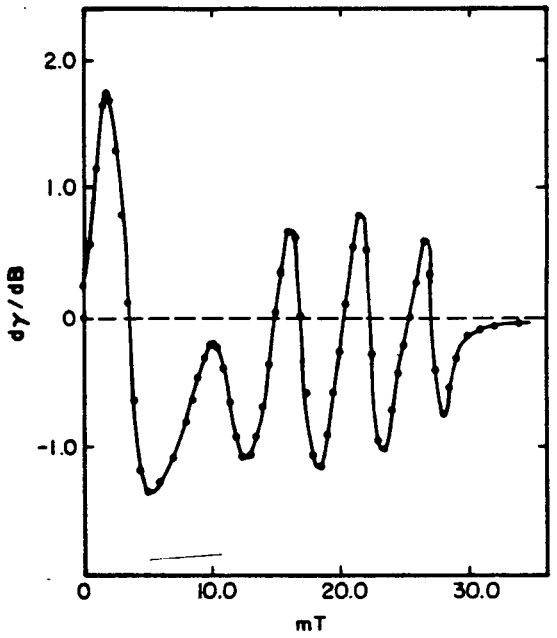

FIG. 4. Synthetic LMR π spectrum of CCH: Computed values of the derivative of the absorption coefficient (arbitrary units), with respect to the external field for $\Delta M_F = 0$ transitions. Half-width $\Delta\nu = 2.0$ MHz.

sorption coefficient with regard to field strength was then computed to enable a direct comparison with the LMR spectrum of Fig. 1. The computation of the synthetic spectrum was carried out with molecular parameters obtained from the microwave[14] and astrophysical data,[3-6] and by use of the g values $g_S = 2.002\,319$, $g_l = 0.003\,042$, and $g_A = g'_R = 0.0$. The only unknown parameter of importance is then the half-width $\Delta\nu$ of Eq. (20). $\Delta\nu$ was adjusted to obtain the best match between the synthetic and observed spectrum, and the optimum value was found to be $\Delta\nu = (2.0 \pm 0.2)$ MHz. The synthesized spectrum for the $M_F = 0$ transition

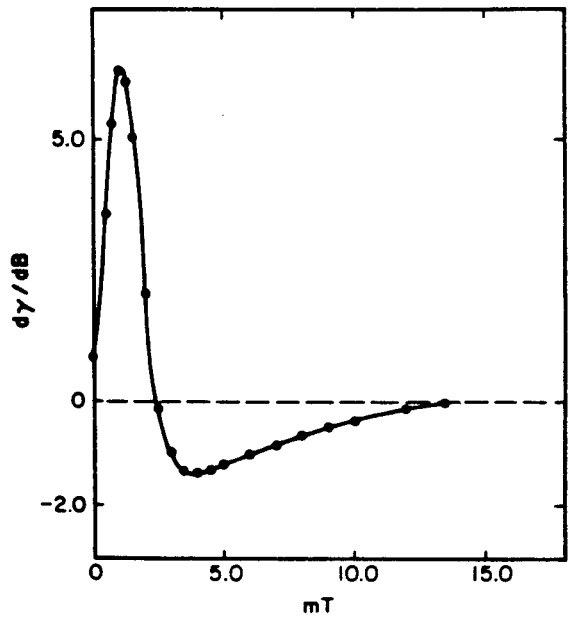

FIG. 5. Synthetic LMR σ spectrum of CCH: Computed derivatives of the absorption coefficient (arbitrary units) for $M_F - M''_F = -1$ transitions. Half-width $\Delta\nu = 2.0$ MHz.

with $\Delta\nu = 2.0$ MHz is shown in Fig. 4, and the spectrum for $M'_F - M''_F = -1$ is shown in Fig. 5, for $\Delta\nu = 2.0$ MHz. The agreement between the synthetic and observed spectra of Fig. 1 is quite good, and it is particularly gratifying that these synthetic spectra were obtained with molecular parameters derived from different rotational transitions, with adjustment of only the half-width $\Delta\nu$.

C. Least-squares determination of the molecular parameters

In order to obtain the best possible description of the $X\,^2\Sigma^+$ state of CCH, the molecular parameters were determined from a weighted nonlinear least-squares fit in which microwave[14] and astrophysical data[3-6] were included simultaneously with the assigned LMR lines of Table I. Unfortunately, no new parameters could be determined from the inclusion of LMR lines, although an improvement in the precision of the known parameters was obtained and the internal consistency of the entire set of high resolution data was verified in this way. In Table II we compare the new fitted parameters with those obtained by Sastry *et al.*,[14] which represented the best parameters previously available.

The values obtained for B_0 in these two separate analyses differ by ~ 150 kHz, while those for D_0 are essentially identical; however, this does not affect the calculated frequencies of high-J transitions, because of the concomitant changes in γ, and in the hyperfine parameters b and c. Moreover, it may at first seem suspicious that the present analysis, based on new LMR data for which hyperfine splittings are unresolved, results in somewhat different values for the hyperfine parameters. This is a result of three factors: First, in this work we have included our new data in a merged fit of all the existing high resolution gas phase data for CCH, while Sastry *et al.* fixed the hyperfine parameters at values obtained from the astronomical studies; hence, simply the effects of parameter correlation are likely to cause small changes in the values of parameters obtained through nonlinear least squares techniques, as the size and nature of the data set is changed. Secondly, we note that three of the four astronomical transition frequencies exhibit positive deviations of essentially the same magnitude; this may reflect a small error in the values used for the VLSR in obtaining rest frequencies from this data. Finally, and most significantly, although the hyperfine splittings are indeed not resolved in our LMR measurements, the line shapes and intensities do indeed depend on these hyperfine splittings and the calculated LMR spectrum changes notably if these are altered. Therefore, even these overlapped LMR spectra do contain

TABLE II. Fitted values (MHz) of the molecular parameters. The numbers in parentheses represent one standard deviation.

	Sastry *et al.* (Ref. 14)	This work
B_0	43 674.5135(54)	43 674.3607(37)
D_0	0.1052(3)	0.105 44(20)
γ	−62.661(16)	−62.713(19)
b	40.40(19)	40.93(18)
c	12.33(11)	11.93(13)

much of the same information exhibited by a fully resolved spectrum; it is, however, rather more difficult to extract it!

For the LMR lines, the mean frequency of the two unresolved hyperfine transitions (cf. Table I) was used in the fit. This mean frequency was obtained by weighing each of the two transition frequencies according to their relative intensity. The computed final (converged) mean frequencies in Table I are seen to deviate from the laser frequency by less than 1 MHz. The microwave and astrophysical lines included in the fit are also shown in Table I. The accuracy of the molecular eigenstates for higher N values previously predicted from microwave and astrophysical data[6] is confirmed here; the improved set of parameters determined here yields essentially identical results for these eigenvalues.

No molecular g factors could be determined from the present LMR lines. The LMR transition frequencies are quite insensitive to reasonable variations of the second order g factors g_A and g_R' [cf. Eqs. (11) and (12)], and also to reasonable deviations of g_s from the free electron value $g_s = 2.002\,319$.

Earlier in the paper, we noted that a frequency pulling experiment indicated that the strong line near zero field exhibited a positive tuning rate $(\partial H/\partial \nu_L)$ for both σ and π spectra, while the four resolved lines in the π spectrum exhibited a negative tuning rate. This is clearly understood by studying the slopes of the transition frequencies in Fig. 3. Initially, all of the transitions are increasing in frequency with increasing field, and hence will shift to higher fields if the laser is blue shifted; however, as the spin decouples at higher fields, the transition frequencies turn over and tune to lower values with increasing field. Thus the *same* transitions are observed twice—with opposite tuning rates.

V. DISCUSSION

From the results of the weighted least-squares fit, we can compare the hyperfine parameters b and c to the corresponding isotropic and dipolar tensor components measured in cryogenic matrix EPR studies of CCH. Graham, Dismukes, and Weltner[11] give

$$A_{\rm ISO} = 1/3(A_\parallel + A_\perp) = 44(1)\ \text{MHz}$$

and

$$A_{\rm DIP} = 1/3(A_\parallel - A_\perp) = 4(1)\ \text{MHz}$$

for an argon matrix, which compare directly with our gas-phase values of 41.96(20) MHz and 3.97(5) MHz for b and $c/3$, respectively. This implies that the environment of an argon matrix causes a 5% increase in the spin density at the hydrogen nucleus, relative to the isolated molecules, while the dipolar term is unchanged to within experimental error. This, in turn, implies that the amount of s character in the H-atom wave function is increased.

The most interesting result of this work is the demonstration that laser magnetic resonance spectra of radicals with very weak spin coupling can indeed be detected, assigned, and analyzed to yield reliable spectroscopic information. In this prototype case, the badly overlapped spectra of a weakly coupled $^2\Sigma$ molecule were accurately reproduced by a computer model which used molecular constants from earlier work and required only the adjustment of the linewidth parameter; the reasonably well-resolved transitions observed were then included in a fit of all existing data on this state to extract an improved set of molecular parameters. In future cases, where little or no previous data exist for the weakly coupled radical observed, the entire overlapped LMR spectrum can be digitized and itself used as input to a nonlinear least-squares fit involving a model for the absorption coefficient [cf. Eq. (20)]. The molecular parameters then can be determined by adjusting them to reproduce the digitized experimental spectrum. The principal difficulty will be that of searching for transitions of these radicals, having rather limited tuning ranges, on the basis of predictions made from *ab initio* calculations. Extension of the theory and computational techniques demonstrated here for this simple case of a $^2\Sigma$ linear molecule to the more complex case of an asymmetric rotor with weak spin doubling are in progress. This will facilitate the reliable prediction and analysis of LMR spectra of polyatomic radicals with weak spin coupling, and should lead to the extraction of useful information on a number of such radicals that are important as reactive intermediates in combustion processes, with the technique of laser magnetic resonance spectroscopy.

ACKNOWLEDGMENTS

This work was supported by the Director, Office of Energy Research, Office of Basic Energy Sciences, Chemical Sciences Division of the U. S. Department of Energy under Contract No. DE-AC03-76SF00098. RJS thanks the NRC for a postdoctoral fellowship, during which the experimental phase of this work was carried out. We thank Dr. Dennis Reuter and Ms. Lucy Ziurys for assistance in the early phases of data analysis, and thank Professor J. M. Brown and Professor R. F. Curl for critical readings of this paper.

[1] K. Hoyermann and R. Sievert, *Seventeenth Symposium (International) on Combustion* (The Combustion Institute, New York, 1978), p. 517.
[2] K. M. Evenson, R. J. Saykally, R. F. Curl, and J. M. Brown, in *Chemical and Biochemical Applications of Lasers*, edited by C. B. Moore (Academic, New York, 1980).
[3] K. D. Tucker and M. L. Kutner, Astrophys. J. **222**, 859 (1978).
[4] K. D. Tucker, M. L. Kutner, and P. Thaddeus, Astrophys. J. **193**, L115 (1974).
[5] A. Watten, E. P. Bozyan, D. G. Garrett, R. B. Loren, and R. L. Snell, Astrophys. J. **239**, 844 (1980).
[6] L. M. Ziurys, R. J. Saykally, R. Plambeck, and N. Erickson, Astrophys. J. **254**, 94 (1982).
[7] S. K. Shih, S. D. Peyerimhoff, and R. J. Buenker, J. Mol. Spectrosc. **74**, 123 (1979).
[8] S. K. Shih, S. D. Peyerimhoff, and R. J. Buenker, J. Mol. Spectrosc. **64**, 167 (1977).
[9] I. H. Hillier, J. Kendrick, and M. F. Guest, Mol. Phys. **30**, 1133 (1975).
[10] E. L. Cochran, F. J. Adrian, and V. A. Bowers, J. Chem. Phys. **40**, 213 (1964).
[11] W. R. M. Graham, K. I. Dismuke, and W. Weltner, Jr., J. Chem. Phys. **60**, 3817 (1974).
[12] D. E. Milligan, M. E. Jacox, and L. Abouaf-Marguin, J. Chem. Phys. **46**, 4562 (1967).
[13] R. J. Saykally and K. M. Evenson, *Proceedings of the Thirty-Third Symposium on Molecular Spectroscopy*, Columbus, OH, June, 1978, Paper FB-8.
[14] K. V. L. Sastry, P. Helminger, A. Charo, E. Herbst, and F. DeLucia,

Astrophys. J. Lett. 251, L119 (1982).
[15]P. G. Carrick, J. Pfeiffer, R. F. Curl, Jr., E. Koester, F. K. Tittel, and J. V. V. Kasper, J. Chem. Phys. 76, 3336 (1982).
[16]D. J. Knight, Rep. Natl. Phys. Lab. 46 (1981).
[17]L. Veseth, J. Mol. Spectrosc. 59, 51 (1976).
[18]L. Veseth, J. Mol. Spectrosc. 63, 180 (1976).
[19]F. Raab, T. Bergeman, D. Lieberman, and H. Metcalf, Phys. Rev. A 24, 3120 (1981).
[20]C. H. Townes and A. L. Schawlow, *Microwave Spectroscopy* (Dover, New York, 1975).